ANGULAR CORRELATIONS IN PROTON-PROTON COLLISIONS PRODUCING A HIGH TRANSVERSE MOMENTUM π^0

K. EGGERT, W. THOMÉ and K.L. GIBONI

III. Physikalisches Institut der Technischen Hochschule, Aachen, Germany

B. BETEV *, P. DARRIULAT, P. DITTMANN, M. HOLDER,
J. KALTWASSER, K.T. McDONALD **, H.G. PUGH *** and
G. VESZTERGOMBI †

CERN, Geneva, Switzerland

T. MODIS and K. TITTEL

Institut für Hochenergie Physik, Heidelberg, Germany

P. ALLEN, I. DERADO, V. ECKARDT, H.J. GEBAUER,
R. MEINKE, O.R. SANDER ††, P. SEYBOTH and S. UHLIG

Max Planck Institut für Physik und Astrophysik, Munich, Germany

In an experiment at the CERN ISR, a streamer chamber detector surrounding one of the intersection regions was triggered on large transverse momentum π^0's by means of an array of lead-glass counters. The directions of charged particles and γ rays converted in lead-oxide plates inside the streamer chamber were measured. Data were taken at a c.m. energy of $\sqrt{s} = 53$ GeV at two production angles of the high p_T π^0 (90° and 53°). They indicate an enhancement of particles mostly in the hemisphere opposite to the π^0. In the 53° data, a shift of this enhancement towards rapidities opposite to the rapidity of the π^0 and confined to a ±30° azimuthal region around the collision plane is observed. In addition, a short-range angular correlation is evidenced between the high p_T π^0 and the other collision products (photons or charged particles). Two-particle correlations between charged particles produced in association with the high p_T π^0 are found similar to those observed in usual collisions.

 * On leave from Institute of Nuclear Research, Sofia, Bulgaria.
 ** Present address: University of Chicago, Illinois, USA.
 *** On leave from University of Maryland, College Park, Md., USA.
 † Visiting Scientist from JINR, Dubna, USSR, on leave from Central Research Institute, Budapest, Hungary.
 †† Now at UCLA, Los Angeles, Calif., USA.

1. Introduction

Since the discovery of the non-exponential fall of the transverse momentum distribution of secondary particles [1] manifold theoretical effort [2] has been devoted to finding the mechanism responsible for this behaviour. Most of this work is concerned with the detailed description of the dependence of the single-particle distribution upon transverse momentum p_T and c.m. energy $\sqrt{s}$. Yet it seems clear that further understanding and discrimination between models will mostly come from an investigation of the properties of particles produced in association with a high p_T particle. Among several others there are two extreme possibilities: either the high p_T particle is a product of a general excitation in the central region — some kind of a high mass cluster or fireball which decays isotropically — or the high p_T particle is produced in a quasi-elastic two-body collision between constituents of the incoming hadrons. In the latter case, one would expect to see a coplanar structure in the distribution of the outgoing particles as a reminiscence of the original collision process. Some such structure is already imposed by momentum conservation, but the number of secondaries is sufficiently large and the energy sufficiently high at the ISR for phase-space effects to play a minor role.

Since the whole phenomenon of high p_T behaviour may indeed be very complex, it seems appropriate to find out from the data themselves which are the most important and most informative features. There are, however, clear limitations to such a programme: it is virtually impossible to measure masses and momenta of all the particles produced, and even then it would be necessary to condense the information into a few parameters. In the first generation experiment described here, we limit ourselves to a measurement of the direction of all charged secondaries and of part of the γ rays produced in association with a high $p_T\pi^0$, using a large solid-angle optical detector and an array of lead-glass counters to trigger on the high $p_T\pi^0$. From these data we extract angular correlations between the π^0 and associated charged particles or γ rays and correlations among the charged particle themselves.

2. Detector

The detector consists essentially of two large streamer chambers for the observation of particle trajectories and of an array of lead-glass counters which provides a trigger on the large $p_T\pi^0$'s (fig. 1). The streamer chambers, positioned above and below the beam pipes, surround an intersection region of the ISR. Apart from the 8 cm gap between the chambers they cover the full solid angle. Each chamber is 50 cm high, 270 cm lang (along the beams) and 125 cm wide (transverse to the beams). Frames of one radiation length thick lead-oxide plates, 230 cm or 100 cm wide and 50 cm high, are inserted in the sensitive volume of the chambers in order to convert γ rays. The converter plates extend over all rapidities and cover ≈50% of the solid angle. The geometry of the sensitive volumes is such that the visible track
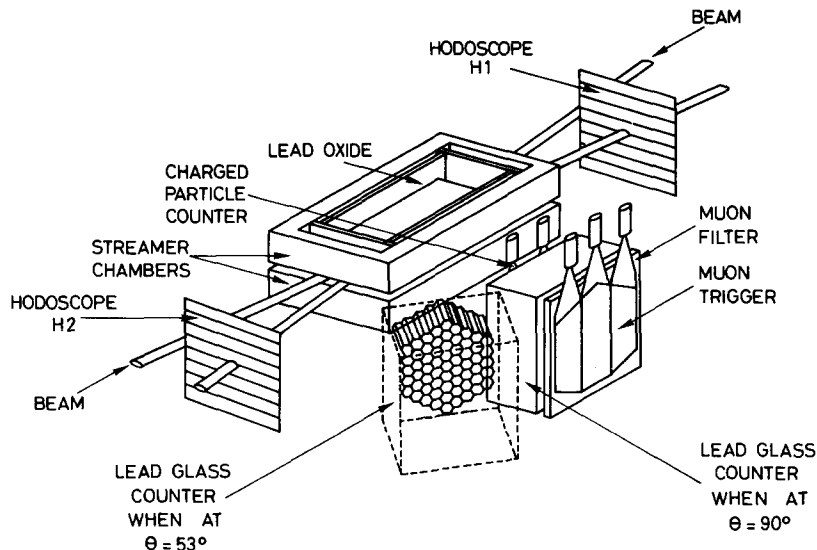
Fig. 1. Schematic view of the set-up.

length is 30 cm in the forward direction and 13 cm on the sides. The angular dependence of the acceptance is governed by the effect of the gap between the chambers for charged particles (fig. 2); for photons it is further limited by the height of the converter plates. The gap causes a $24°$ to $48°$ loss in azimuthal coverage (full range $360°$) as the production angle varies from $90°$ to $10°$. Tracks are photographed through two $8°$ stereo views and recorded on a single 35 mm film.

The lead-glass detector [3] is a $1m^2$ hexagon comprising 61 hexagonal blocks, each 13.5 cm in diameter, 15 radiation lengths deep and viewed by a 5 inch phototube. It was located at c.m. angles of $90°$ (or $53°$), at a distance of 1.90 m (or 2.60 m) from the intersect, and its centre was 56 cm below the beam level to match the acceptance of the streamer chamber. The pulse heights of the anode signals of each cell were analysed in 8 bit ADC units and recorded on magnetic tape. A more complete description of the apparatus is given elsewhere [4]. The performance of the lead-glass detector is discussed in another paper [5].

The chambers were triggered whenever the sum of the lead-glass counter dynode signals exceeded an adjustable threshold and was in coincidence with a signal from two large downstream scintillator hodoscopes.

In a series of runs, referred to as minimum bias triggers, only the scintillation counters were used in the trigger. The cross section seen by the scintillators is 37 mb at $\sqrt{s} = 53$ GeV [6].
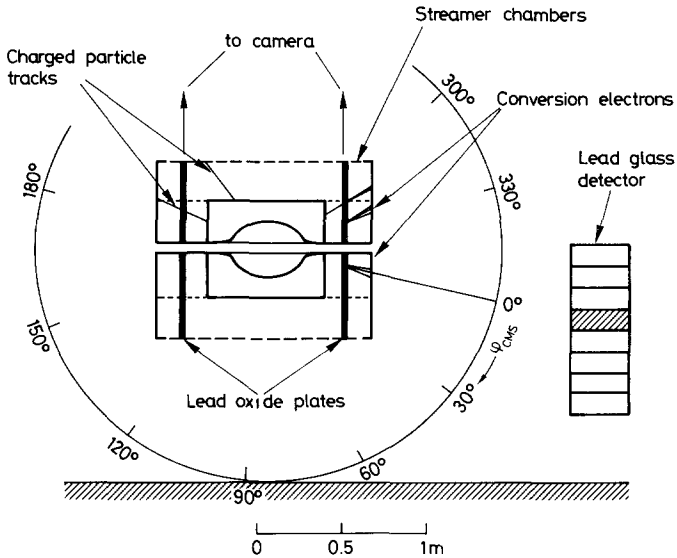
Fig. 2. Cross section of streamer chambers and lead-glass perpendicular to the beam direction. The π^0 which has triggered the lead-glass detector defines the zero of azimuthal angle.

3. Data reduction and analysis

The data analysis consists of two separate parts: processing of the lead-glass information and measurement of the pictures. Details of the lead-glass pattern recognition are discussed in ref. [5]. Relevant to our purpose is that we may neglect energy corrections due to escape of one of the π^0 decay photons, or due to an extra, uncorrelated particle which overlaps the shower of the π^0. The pictures are scanned and measured on image plane digitizing projectors. Three points are measured in each view on all tracks which point into the civinity of the interaction region. The setting error is about 12 μm on film (2 mm in space).

Tracks are reconstructed as straight lines in space using the two stereo views. Typical uncertainties of the track extrapolation to the interaction region are 0.6 cm (8 cm) in the horizontal (vertical) projection. The interaction point is found by an iterative least squares fit to the measured tracks. The resulting errors on the final vertex position are about 0.3 cm in the horizontal plane, and 4 cm along the vertical direction. All tracks pointing to the vertex within three standard deviations are accepted, and their directions in space are recalculated using the interaction vertex as an additional constraint. In this last step, the vertex is assumed to lie in the plane of the beams, as the heights of the beams are much smaller than vertical reconstruction uncertainties, and their positions are accurately known.

In the absence of momentum measurement and particle identification, each track

Table 1
Data samples

90° data			53° data		
p_T range (GeV/c)	$\langle p_T \rangle$ (GeV/c)	Number of events	p_T range (GeV/c)	$\langle p_T \rangle$ (GeV/c)	Number of events
<1.4	0.85	840	3.0–5.0	3.8	1196
1.4–2.5	2.1	799			
2.5–3.5	3.0	1339			
3.5–4.5	3.85	715			
>4.5	5.1	180			

is completely described by its azimuth ϕ and production angle θ. These quantities are calculated in the laboratory system and transformed to the c.m. system under the assumption that the produced particles have zero mass. Because of the small crossing angle (15°) of the beams, this approximation has no important effect on the analysis. We also approximate the rapidity $y = -\frac{1}{2} \log[(E - p_L)/(E + p_L)]$ by $\eta = -\log \tan(\frac{1}{2}\theta)$. Typical uncertainties due to reconstruction errors are 5° in ϕ and 0.1 units in η for charged tracks, and 15° in ϕ, 0.1 units in η for converted γ rays.

Rescans were made for about $\frac{2}{3}$ of the sample. We estimate the track loss in scanning and reconstruction to be 8% for charged particles and 18% for γ rays. The higher loss rate for γ rays is mainly due to problems of overlap with other γ rays and charged particles produced in the lead-oxide plates. The fractional loss does not depend on production angle. The data have not been corrected for the loss in charged particles. In order to compare γ and charged particle distributions, the γ distributions have been scaled up by 10%.

We report here on data taken at a c.m. energy of $\sqrt{s} = 53$ GeV, with two positions of the lead-glass counter, at mean c.m. production angles of 90° and 53°. We have analysed data in various p_T intervals at $\theta = 90°$, but only around $p_T = 3.8$ GeV/c for $\theta = 53°$ (table 1).

4. Acceptance calculattions

The acceptance for charged particles was calculated by a Monte-Carlo simulation of events using realistic multiplicity distributions, and single-particle spectra as observed with minimum bias trigger. Measurement errors, multiple scattering and nuclear interactions in the vacuum chamber walls or in the streamer chamber material were taken into account. π^0's were created in the simulation programme with the same spectra as charged pions and in the proportion 1 : 2. From conversion of γ rays or Dalitz decays of π^0's one expects between 3% and 10% additional tracks, depending on the rapidity interval. Both charged pions from K_s^0 decays will normal-

ly be accepted; in about 30% of the decays it is possible to reject at least one of the pions as not pointing to the interaction vertex. This figure is almost independent of the K momentum. No correction for these additional sources of charged particles is made. Except for the regions around the gap between the streamer chambers the acceptance is always greater than 90%. A 4% systematic error is attributed to this calculation, which allows for differences in the measurement accuracies and uncertainties in the Monte-Carlo input data.

Tracks are weighted with the inverse of their acceptance probability. The effect of the gap between the chambers in high p_T data is taken into account by assuming that the particle distribution in a $\Delta\phi = \pm20°$ interval including the gap ($\Delta\phi = \pm6°$ for $\eta < 2$) is flat. This assumption is justified by the observation that for any fixed direction of a track the difference in azimuth to the π^0 varies from event to event by $\pm10°$ due to different locations of the π^0 in the lead-glass counter.

In the angular region covered by the lead-glass counter it is important to avoid any trigger bias. For the study of correlations alongside the π^0 a very restrictive cut on the π^0 energy is applied, excluding events in which the π^0 itself does not have sufficient energy to trigger, but another particle hitting the lead-glass detector supplies additional energy. Even though this energy is usually small (around 200 MeV), the probability of such a configuration is enhanced in the trigger due to the steeply falling π^0 spectrum. About $\frac{1}{3}$ of the analysed events are eliminated by the cut.

Charged particles which point towards the π^0 cluster in the lead-glass are removed from the remaining events. Their frequency (≈0.25 tracks per event) is in agreement with expectations: 0.17 are due to photons from the decays of the high $p_T\pi^0$ converting in the aluminium base plate of the chamber, 0.04 are due to accidental overlaps between charged particles and the π^0, and 0.05 are mismatches due to finite resolution in the track reconstruction. To correct for this last effect, 0.05 tracks per event are added to the sample at the end.

The acceptance calculations for γ rays observed behind the lead-oxide plates follow the same principles, except that γ rays are additionally weighted with the inverse of the conversion probability. The weights depend on the thickness of the material traversed and are energy independent above 200 MeV. In the range 30–200 MeV, the energy dependence of the conversion probability was measured for lead-oxide plates of one and two radiation lengths thickness, using a scintillation counter set-up in a tagged photon beam at the CERN Synchro-cyclotron [7]. Since the energies of individual γ rays observed in the streamer chamber are not known, only a global correction factor for this low-energy effect is introduced, based on published γ spectra [8]. The correction is 20% for rapidities less than 1 and vanishes for rapidities greater than 2. In high p_T trigger data, where the associated γ spectra are not known, only half of this correction was applied, with an uncertainty of the same size. An average loss of 8% of γ rays was taken into account in a $\pm30°$ ϕ interval including the gap between the chambers due to photons converting in the base plate and appearing as charged tracks.
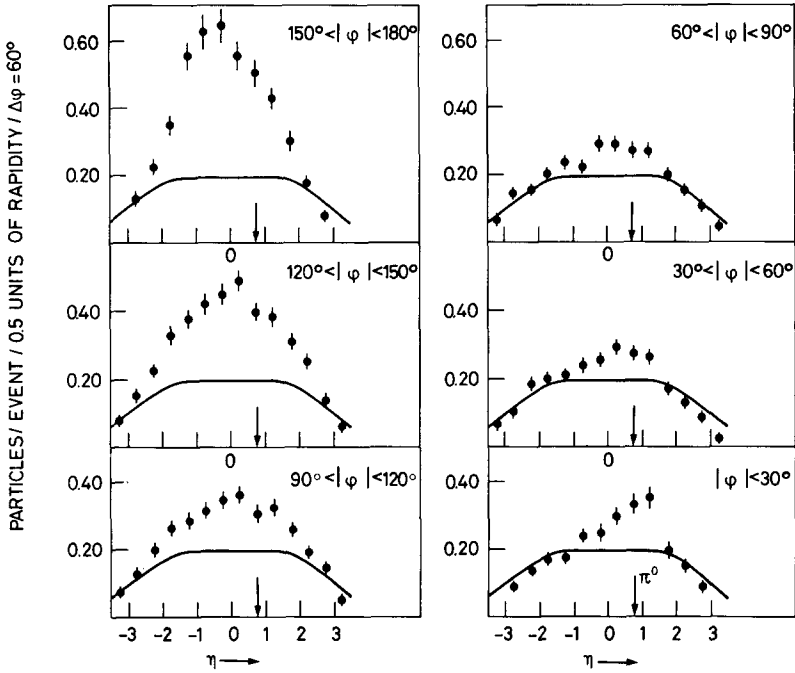
Fig. 3. Charged particle densities for the 53° data. The solid lines give charged particle densities in minimum bias triggers.

5. Correlations between the high p_T π^0 and charged particles

The average charged particle distribution in events with a high p_T π^0 is given as a function of rapidity and azimuth as

$$\frac{dN}{d\eta d\phi} = \frac{1}{\sigma'} \frac{d\sigma'}{d\eta d\phi} \, ,$$

with the normalization

$$\int \frac{dN}{d\eta d\phi} \, d\eta d\phi = \langle n \rangle \, ,$$

where σ' is the cross section for observing a π^0 in a given interval of p_T, and $\langle n \rangle$ is the average multiplicity of charged particles in such events. The azimuth is measured in the c.m. system with respect to the plane containing the beam direction and defined for each event such that the π^0 has zero azimuth angle (fig. 2). We give then particle distributions in ϕ bins of 30°, adding the distributions for positive and negative ϕ's.
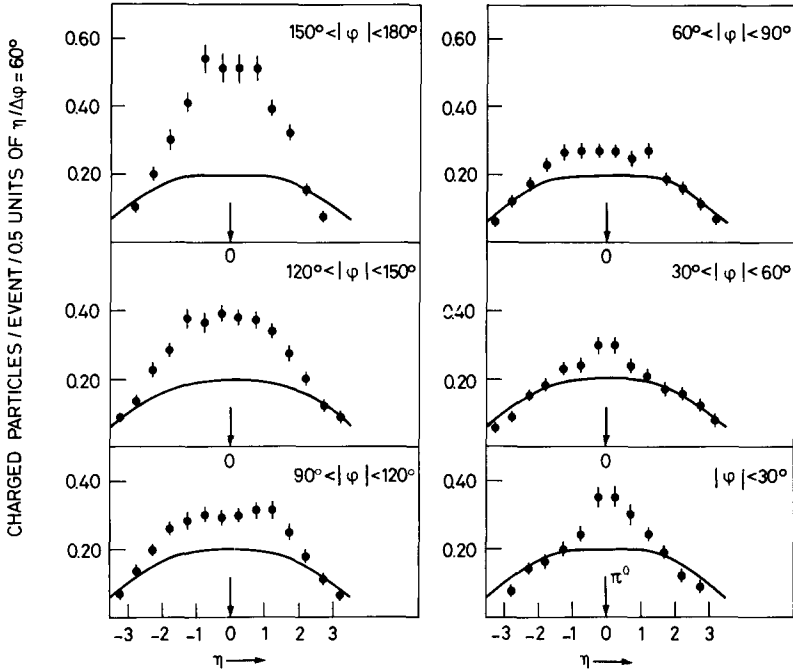
Fig. 4. Charged particle densities for the 90° data, averaged over events with p_T of the π^0 > 2 GeV/c. The solid lines give charged particle densities in minimum bias triggers.

We first discuss the 53° data $[\eta(\pi^0) = 0.75]$, which have the advantage that a correlation between the high $p_T\pi^0$ and associated particles will show up as an asymmetry in the rapidity distribution. In fact, a shift towards rapidities opposite to that of the π^0 has been previously reported for particles in the opposite hemisphere from earlier data of this experiment [9] and by the Pisa-Stony Brook Collaboration [10]. The 53° data allow us to study this effect further. They show several interesting features (fig. 3):

(i) an enhancement in the same azimuthal region as the $\pi^0(|\phi| < 30°)$ which is centred at the same rapidity as the π^0 and which has a relatively short range in rapidity (about ±0.7 units);

(ii) an increase of particle density over the whole central region ($|\eta| \leqslant 2$), in the opposite hemisphere ($|\phi| > 90°$), most prominent for azimuthal angles near 180°;

(iii) an asymmetry of the rapidity distribution in a $\Delta\phi = \pm 30°$ sector around $\phi = 180°$.

For comparison, the distributions of charged particles in interactions with minimum bias trigger which contain at least two particles in the streamer chamber are also shown in fig. 3.
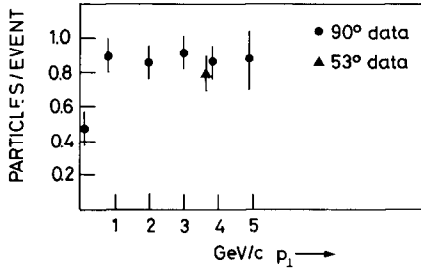
Fig. 5. Charged particles involved in the short-range correlation with the high $p_T \pi^0$. Particle densities were integrated over $|\eta - \eta_{\pi^0}| < 1.5$, $|\phi| < 60°$ and the corresponding densities in minimum bias triggers were subtracted.
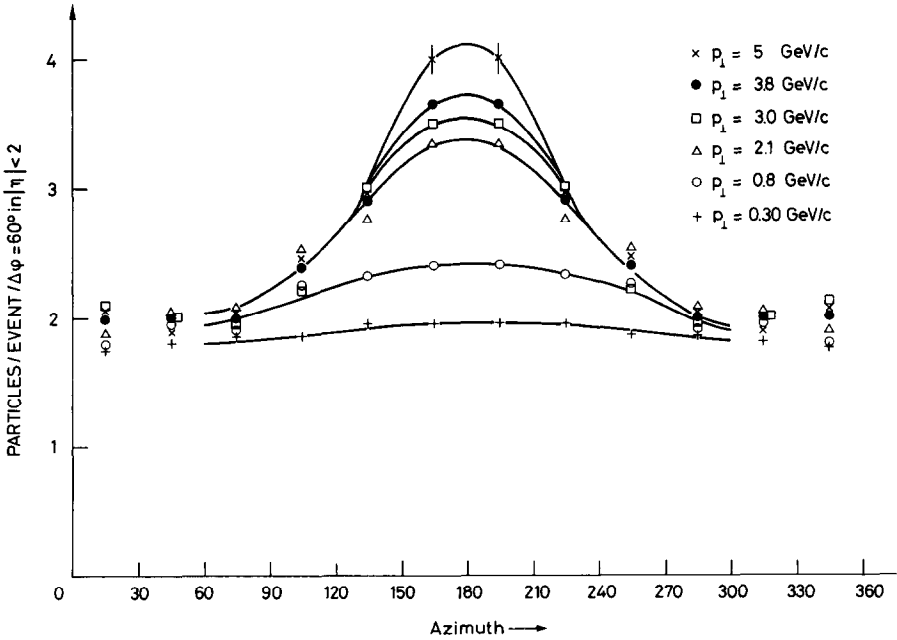

Fig. 6. Azimuthal distribution of charged particle densities integrated over $|\eta| < 2$ as a function of p_T of the π^0 for the 90° data. The lines are handdrawn curves through the data. The data are symmetrized around $\phi = 180°$ to reduce the statistical errors. A typical error bar is shown for the $p_T = 5$ GeV/c data.
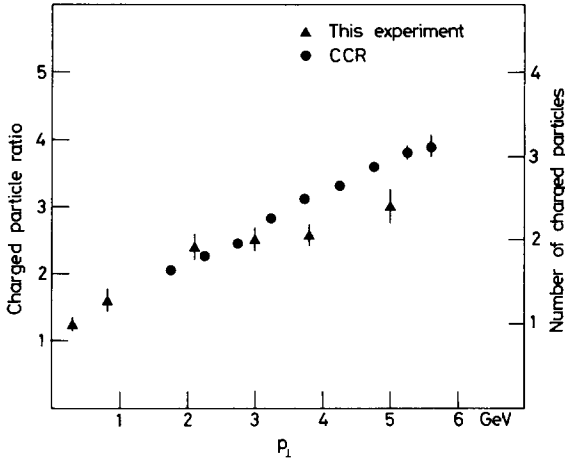
Fig. 7. Charged particle densities, integrated over $|180° - \phi| < 30°$, $|\eta| < 1$ as a function of p_T (right-hand scale). For a comparison with the data of ref. [12] we give also the ratio to minimum bias triggers (left-hand scale). In the CCR experiment the charged particle ratios are given for the interval $|180° - \phi| < 23°$, $|\eta| < 0.8$. The definition of minimum bias triggers is not exactly the same in the two experiments.

Each of these observations merits some discussion.

(i) A similar short range enhancement around the π^0 direction is observed in the 90° data where it is symmetric around $\eta = 0$, as is to be expected (fig. 4). In order to study the p_T dependence of this correlation we integrate the particle density in a $\Delta\eta = \pm1.5$, $\Delta\phi = \pm60°$ interval around the π^0 and subtract, somewhat arbitrarily, the same quantity deduced from minimum bias interactions. This also provides an estimate, to within 30%, of the average number of particles involved in this correlation. The results are shown in fig. 5. A low-energy point has been included, from data where the lead-glass counter was not used in the trigger, but where a photon was observed in the streamer chamber in the interval $|\eta| < 0.5$. Apart from this low-energy point, which represents the correlation between γ rays and charged particles at low momenta, there is no p_T dependence of the correlation within measurement errors. The average number of correlated charged particles in the indicated interval of rapidity and azimuth is 0.85 ± 0.15, where the error is only statistical. Restricting the ϕ interval to $|\phi| \leqslant 30°$, this number would be 0.50 ± 0.10, with the same p_T (in-)dependence.

(ii) The particle density in the opposite hemisphere, as first observed by the Pisa-Stony Brook Collaboration [11] increases with the transverse momentum of the π^0. The extension in rapidity of this increase does not vary for the observed range in p_T within our measurement errors. Fig. 6 shows the ϕ dependence of the particle density, integrated in η from -2 to $+2$, for the 90° data. The increase with p_T is strongest

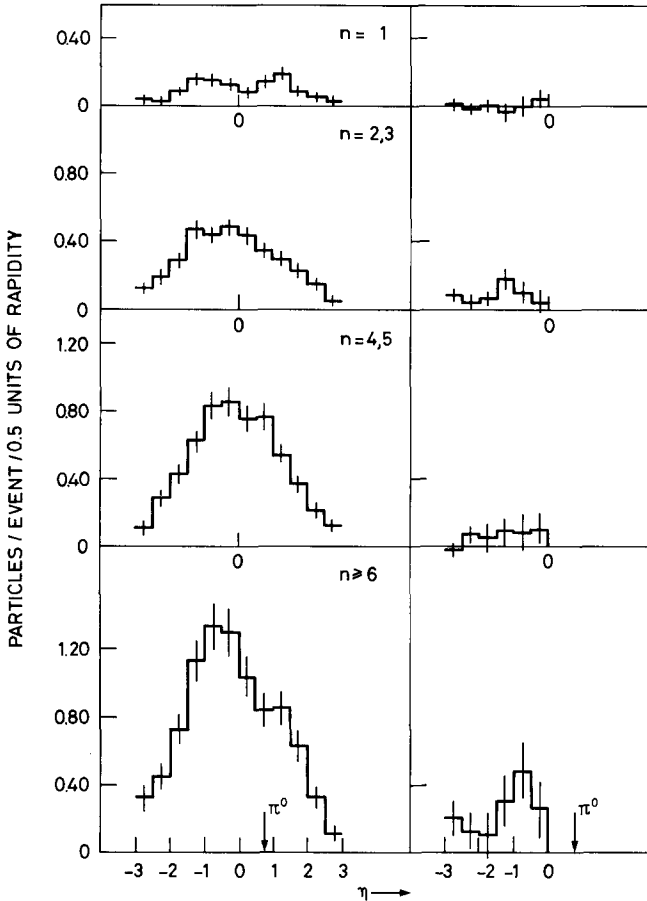Fig. 8. Charged particle rapidity distributions in the interval $|\phi - 180°| < 30°$ as a function of the multiplicity in this interval. The right half of the figure displays the asymmetry (particle density in an interval at negative rapidity minus particle density in the corresponding interval at positive rapidity.

in the neighbourhood of $\phi = 180°$, where the data are compatible with a linear increase up to the largest p_T of 5 GeV/c (see fig. 7). For comparison we also show the data of Büsser et al. [12].

(iii) The distribution of particles in the 53° data is symmetric in rapidity over most of the ϕ region (fig. 3): the particles in the hemisphere opposite to the π^0, which must be involved in the momentum balance, neither follow the longitudinal motion of the π^0 nor cluster around the opposite rapidity. Only in the $\Delta\phi = \pm30°$
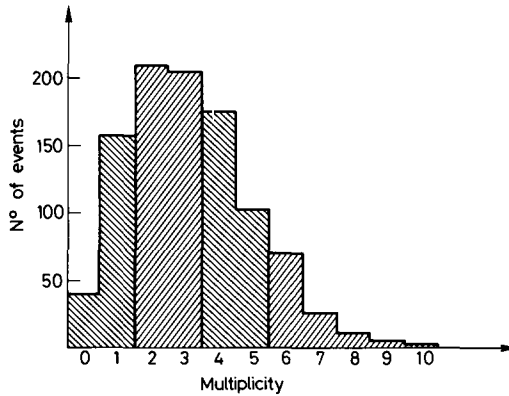
Fig. 9. Distribution of the charged particle multiplicities in the interval $|\phi - 180°| < 30°$. The multiplicity bins are those chosen for fig. 8.

interval around 180° there is a small but significant asymmetry. It is possible to regard this effect as a superposition of a symmetric distribution, as observed in other ϕ intervals, and an asymmetric component. Then this asymmetric component is concentrated around the rapidity opposite to that of the π^0 and contains an average of 0.50 ± 0.12 particles per event.

It is interesting to see how this asymmetry varies with the charged particle multiplicity in the $|\phi - 180°| < 30°$ interval, the one which exhibits the asymmetry. One can see (fig. 8) that the asymmetry is largely due to events with high multiplicities. Such events are relatively rare (fig. 9). The interpretation of this observation is not straightforward. For example, it may be that a large fraction of the π^0 momentum is balanced by a single object which subsequently decays into the observed particles, in which case an asymmetry would be more apparent for larger multiplicity of the decay products. While momentum conservation may cause some asymmetry of the rapidity distribution it is surprising that the observed asymmetry is confined to a relatively narrow interval around the collision plane. We have checked that the absence of asymmetry in the next ϕ interval $(30° < |180° - \phi| < 60°)$ persists if we select events with high multiplicity in the previous intervals $(|180° - \phi| < 30°)$ or with high multiplicity in the same interval. Data at lower values of p_T, which should show how this asymmetry builds up as a function of p_T, are not yet analysed.

6. Correlations between π^0 and photons

Analogous distributions to those discussed in the preceding paragraphs can be made for γ rays observed in high p_T events. The ϕ acceptance is, however, limited to
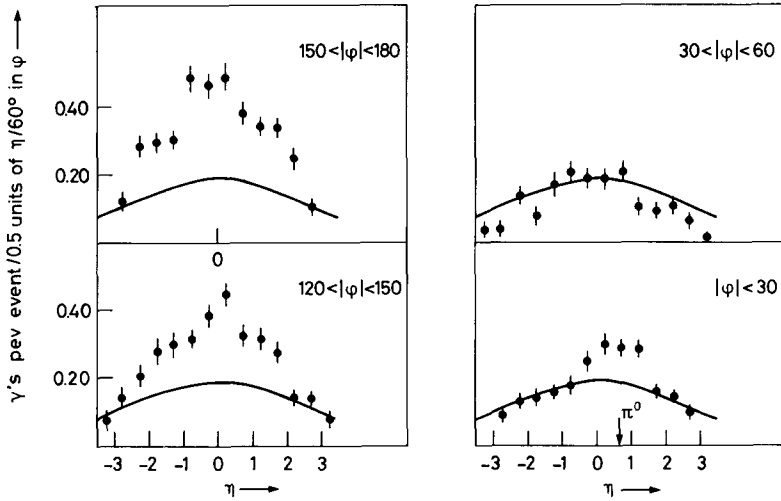
Fig. 10. Gamma ray densities for the 53° data. The solid lines are γ ray densities observed with minimum bias triggers.

the ϕ intervals $-60° \leqslant \phi < 30°$ and $120° \leqslant \phi < 210°$ (fig. 2) due to the limited extension of the lead-oxide plates. As discussed above, the corrections due to losses, either in the scanning or by early conversions of the photons, are larger than for charged particles and there is some uncertainty in the average conversion probability, since the spectrum of photons is unknown. Finally, the errors in the reconstructed γ directions are larger, since the conversion electrons do not point to the interaction vertex, and their origin on the lead-oxide plates is only visible in one of the stereo views, but obscured on the other by the lead-oxide.

Measurements of γ rays are available for the 53° data and for minimum bias triggers.

The γ rays show a similar behaviour to that of the charged particles (fig. 10).

(i) In minimum bias triggers the distribution of γ rays and charged particles are the same within errors.

(ii) In the events with high p_T trigger there is a clear correlation with the π^0 in the $\pm 30° \phi$ interval around the π^0.

(iii) There is an increase in particle density in the opposite hemisphere similar to that observed for charged particles.

(iv) An asymmetry in the rapidity distribution in the $\pm 30° \phi$ interval around $\phi = 180°$ is less evident than in the case of charged particles.

The most prominent feature is certainly the correlation within $\Delta\phi = \pm 30°$ and $\Delta\eta = \pm 1$ with the π^0. The number of photons involved in that correlation, estimated by subtracting the distribution of photons obtained in minimum bias triggers, is
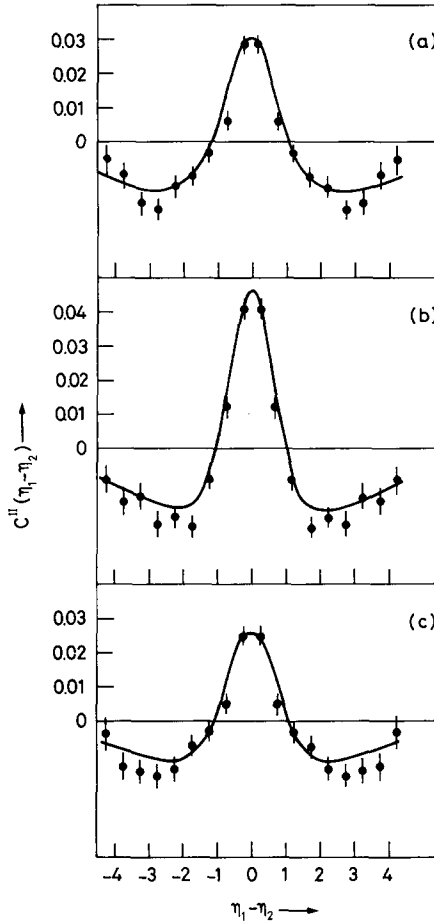
Fig. 11. Two-particle correlation functions, as defined in the text for (a) minimum bias triggers, $|\phi| < 90°$, (b) high p_T triggers with $p_T > 2$ GeV/c in the 90° data, $|\phi| > 90°$, (c) high p_T triggers with $p_T > 2$ GeV/c in the 90° data, $|\phi| < 90°$. The curves are the best fits to a parametrization according to eq. (1).

0.35 ± 0.10 per event. Photons from the decay of the high $p_T \pi^0$ do not contribute to this correlation; the opening angle is so small that the photons point within errors to the triggering lead-glass cluster and are therefore removed from the sample by the cuts described above. A total of 0.06 ± 0.03 γ rays are estimated to be due to η decays [5,13]. From $K_s^0 \to 2\pi^0$ decays one expects a contribution of 0.06 ± 0.02 γ rays per event, using the published value of K^+/π^+ and K^-/π^- ratios at high p_T [14]. The remaining correlation, 0.23 ± 0.11 γ rays per event, is smaller than the correlation involving charged particles.
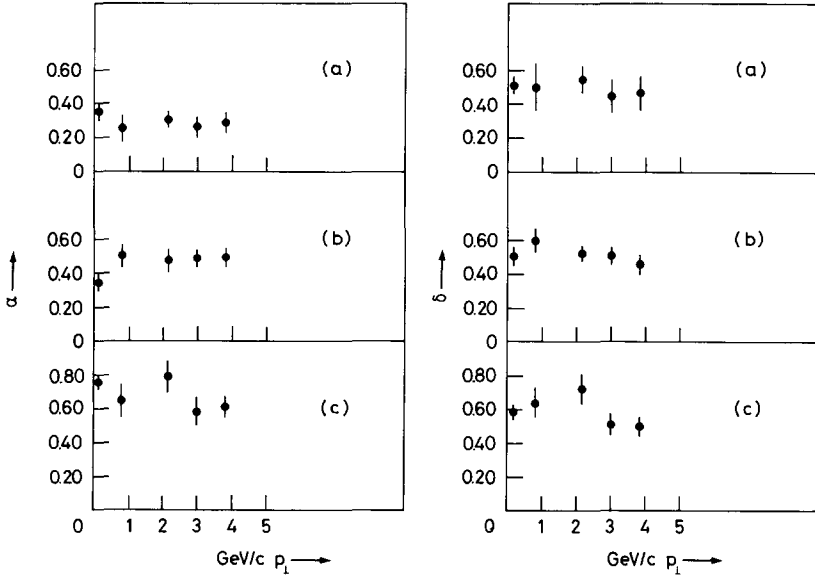
Fig. 12. Parameters describing the two-particle correlation as a function of $p_T(\pi^0)$ for the 90° data (see text): (a) opposite hemisphere, (b) same hemisphere, (c) both hemispheres.

7. Correlation among charged particles

Charged products of proton-proton collisions are known to exhibit an important short-range correlation between two particles. The analysis of the rapidity and azimuthal structure of this correlation in the central rapidity plateau [15] suggests that production of low-mass resonances, like ρ, ω, etc., may play an important role. It is interesting to study these correlations as a function of p_T. We use the formalism developed earlier for low p_T events [15], as a convenient way to parametrize the data.

The two-particle correlation for fixed multiplicity n in the interval $-\eta_{max} < \eta < \eta_{max}$, defined as

$$C_n^{II}(\eta_1, \eta_2) = \rho_n^{II}(\eta_1, \eta_2) - \rho_n^I(\eta_1)\rho_n^I(\eta_2) ,$$

with

$$\rho_n^{II}(\eta_1, \eta_2) = \frac{1}{n(n-1)\sigma_n} \frac{d^2\sigma_n}{d\eta_1 d\eta_2} ,$$

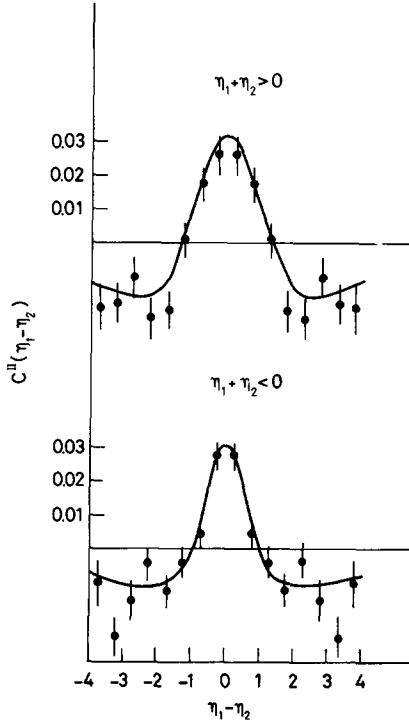$$\rho_n^I(\eta_1) = \frac{1}{n\sigma_n} \frac{d\sigma_n}{d\eta_1} ,$$

Fig. 13. Two-particle correlation functions for two regions of $\eta_1 + \eta_2$ in the hemisphere oppo-site to the π^0 for the 53° data. The curves are the best fits to a parametrization according to eq. (1).

$$\int \rho_n^{\mathrm{II}}(\eta_1, \eta_2)\mathrm{d}\eta_1\mathrm{d}\eta_2 = 1 ,$$

$$\int \rho_n^{\mathrm{I}}(\eta_1)\mathrm{d}\eta_1 = 1 ,$$

$$\int C_n^{\mathrm{II}}(\eta_1, \eta_2)\mathrm{d}\eta_1\mathrm{d}\eta_2 = 0 ,$$

is decomposed into two terms, a Gaussian in rapidity difference describing the short-range correlation, and the product of the uncorrelated particle densities

$$C_n^{\mathrm{II}}(\eta_1, \eta_2) = \frac{\alpha_n}{n-1}\left\{\Gamma^2(\eta_1 - \eta_2) - \rho_n^{\mathrm{I}}(\eta_1)\rho_n^{\mathrm{I}}(\eta_2)\right\} ,$$

where

$$\Gamma^2(\eta_1, \eta_2) \propto \exp\left[\frac{-(\eta_1 - \eta_2)^2}{4\delta^2}\right],$$

Table 2
Correlation parameters

Azimuthal region	$|\phi| < 90°$		$|\phi| > 90°$		all ϕ	
Multiplicity interval	$4 \leqslant n \leqslant 12$		$4 \leqslant n \leqslant 12$		$6 \leqslant n \leqslant 20$	
Rapidity interval	$-2.5 < \eta < 2.5$		$-2.5 < \eta < 2.5$		$-2.5 < \eta < 2.5$	
p_T (GeV/c)	α	δ	α	δ	α	δ
0.3	0.36 ± 0.03	0.52 ± 0.05	0.36 ± 0.03	0.52 ± 0.05	0.59 ± 0.03	0.76 ± 0.04
0.85	0.25 ± 0.08	0.50 ± 0.14	0.51 ± 0.07	0.60 ± 0.07	0.65 ± 0.10	0.64 ± 0.09
2.1	0.31 ± 0.04	0.55 ± 0.08	0.48 ± 0.04	0.53 ± 0.04	0.80 ± 0.10	0.73 ± 0.08
3.0	$0.26 \pm 0 06$	0.44 ± 0.10	0.48 ± 0.05	0.51 ± 0.05	0.58 ± 0.06	0.51 ± 0.06
3.85	0.30 ± 0.07	0.40 ± 0.11	0.49 ± 0.06	0.45 ± 0.06	0.61 ± 0.06	0.50 ± 0.05

with the normalization

$$\int_{|\eta| < \eta_{max}} \Gamma^2(\eta_1, \eta_2) d\eta_1 d\eta_2 = 1 \ .$$

As in the case of minimum bias triggers, it turns out that α_n does not depend on n within errors, so that an average

$$C^{II}(\eta_1, \eta_2) = \langle (n - 1) C_n^{II}(\eta_1, \eta_2) \rangle = \alpha \{ \Gamma^2(\eta_1 - \eta_2) - \rho^I(\eta_1)\rho^I(\eta_2) \} \qquad (1)$$

can be formed. Since we are interested in the dependence of C^{II} on $\eta_1 - \eta_2$, we will average C^{II} over $\eta_1 + \eta_2$.

We study the rapidity correlation for three intervals of azimuth: $0° \leqslant |\phi| \leqslant 90°$ (the hemisphere of the large $p_T\pi^0$), $90° \leqslant |\phi| \leqslant 180°$ (the opposite hemisphere) and both hemispheres together, denoting by n the charged-particle multiplicity in the corresponding ϕ interval. Fig. 11 shows the two-particle correlation functions $C^{II}(\eta_1 - \eta_2)$ for the two hemispheres for the 90° data with $p_T \geqslant 2$ GeV/c, and for minimum bias triggers. Selection on multiplicity and rapidity intervals are indicated in table 2. The best fit parameters describing the raw data are also given in table 2 and displayed in fig. 12. The dependence of α and δ on p_T is weak. Since the multiplicity in the hemisphere opposite to the π^0 almost doubles between $p_T = 0$ and $p_T = 4$ GeV/c, this implies that the additional particles are correlated with similar strength as the particles in minimum bias triggers.

In order to study the dependence of C^{II} on $\eta_1 + \eta_2$, we use the 53° data. There one can compare the correlation function $C^{II}(\eta_1 + \eta_2)$ for particles in the opposite hemisphere in the interval $\eta_1 + \eta_2 < 0$ and $\eta_1 + \eta_2 > 0$ (fig. 13). The former inter-

val contains mainly the short-range correlation among particles which are also opposite in rapidity to the π^0. The correlation seems to be narrower in this interval; the effect is not, however, sattistically significant. The probability that the two distributions in fig. 13 agree is 8%.

It is tempting to comment on these observations. The symmetric distribution in rapidity for most of the particles in the 53° data suggests that these particles are not strongly correlated in longitudinal momentum with the high p_T particle, yet the asymmetry in azimuth indicates that they are involved in the transverse momentum balance. It is instructive to estimate which azimuthal asymmetry would be observed if all particles were decay products of low-mass resonances and if the transverse momentum of the trigger π^0 were equally balanced among those. To this effect, we have considered a simple model, where ρ, ω and η mesons are produced with invariant cross sections proportional to $\exp(-4p_T)$. The cloud of mesons is assumed to recoil against the π^0 to balance the transverse momentum. It turns out that the actually observed azimuthal asymmetry is smaller than any mixture of ρ, ω, and η mesons can produce. In addition, the model generates stronger correlation among particles in the hemisphere opposite to the trigger π^0 than among particles in the π^0 hemisphere, in contradiction with observation. This may imply that a large fraction of the π^0 transverse momentum is balanced by only a few particles.

8. Conclusion

We have taken advantage of the large coverage and excellent resolution of our streamer chamber detector to improve the knowledge of the structure of large transverse momentum events. The angular configuration of the collision products is observed over a very large solid angle, but without momentum measurement. In spite of its limited scope, this experiment has revealed several new features, which may be schematically summarized as follows:

(i) a broad enhancement of particle density is observed for both charged products and γ rays. This enhancement is centred around rapidity zero and azimuth opposite to that of the large $p_T\pi^0$, and extends approximately over ±2 units of rapidity and ±90° in azimuth, independently of p_T. In this angular region, the number of charged particles increases by 3.7 ± 0.3 between $p_T = 0.3$ GeV/c and $p_T = 5$ GeV/c;

(ii) a second component, extending over a relatively short angular range around the high transverse momentum π^0, is observed for both γ rays and charged particles. In a domain $|\Delta\eta| < 1.5$, $|\Delta\phi| < 60°$, it contains 0.85 ± 0.15 charged particles, independent of p_T;

(iii) in the data where the high $p_T\pi^0$ is produced at 53°, a third component, confined to a narrow azimuthal range ($|\Delta\phi| < 30°$), and centred around a direction opposite to that of the large $p_T\pi^0$, is clearly evidenced from an asymmetry in the density of charged particles, and to a lesser extent in that of γ rays. It contains an average of 0.50 ± 0.12 charged particles per event. A colinear structure, as implied by

this last observation, may be expected if hard scattering of proton constituents is at the origin of the high p_T collision.

The reduction of the collision products to three different components is, however, largely arbitrary. To answer the question of the physical significance of such a description requires more refined measurements with momentum analysis and particle identification. Such measurements would permit a critical comparison with predictions of those models which can qualitatively accomodate our present observations, such as hard scattering models of proton constituents [2] or hadronic bremsstrahlung models [16].

References

[1] F.W. Büsser, L. Camilleri, L. Di Lella, G. Gladding, A. Placci, B.G. Pope, A.M. Smith, J.K. Yoh, E. Zavattini, B.J. Blumenfeld, L.M. Lederman, R.L. Cool, L. Litt and S.L. Segler, Phys. Letters 46B (1973) 471;
B. Alper, H. Bøggild, G. Jarlskog, G. Lynch, J.M. Weiss, P. Booth, L.J. Carroll, J.N. Jackson, M. Prentice, G. von Dardel, L. Jonsson, G. Damgaard, K.H. Hansen, E. Lohse, F. Bulos, L. Leistam, A. Klovning, E. Lillethun, B. Duff, F. Heymann and D. Quarrie, Phys. Letters 44B (1973) 521;
M. Banner, J.L. Hamel, J.P. Pansart, A.V. Stirling, J. Teiger, H. Zaccone, J. Zsembery, G. Bassompierre, M. Croissiaux, J. Gresser, R. Morand, M. Riedinger and M. Schneegans, Phys. Letters 44B (1973) 537.
[2] S.D. Ellis, Proc. 17th Int. Conf. on high-energy physics, London, 1974 (Rutherford Lab., Chilton, Didcot, 1974) p. V-23.
[3] M. Holder, E. Radermacher, A. Staude, P. Darriulat, J. Deutsch, J. Pilcher, C. Rubbia, K. Tittel, C. Grosso-Pilcher, M. Sciré and A. Villari, Nucl. Instr. 108 (1973) 541.
[4] K. Eggert, W. Thomé, B. Betev, G. Bohm, P. Darriulat, P. Dittmann, E. Gygi, M. Holder, K.T. McDonald, T. Modis, H.G. Pugh, F. Schneider, H. Albrecht, K. Tittel, I. Derado, V. Eckardt, H.J. Gebauer, R. Meinke, O.R. Sander and P. Seyboth, Nucl. Instr. 126 (1975) 477.
[5] K. Eggert, K.L. Giboni, W. Thomé, B. Betev, P. Darriulat, P. Dittmann, M. Holder, K.T. McDonald, T. Modis, H.G. Pugh, G. Vesztergombi, K. Tittel, V. Eckardt, H.J. Gebauer, R. Meinke, O.R. Sander and P. Seyboth, Nucl. Phys. B98 (1975) 49.

[6] K. Eggert, H. Frenzel, K.L. Giboni, W. Thomé, B. Betev, P. Darriulat, P. Dittmann, M. Holder, K.T. McDonald, T. Modis, H.G. Pugh, K. Tittel, V. Eckardt, H.J. Gebauer, R. Meinke, O.R. Sander and P. Seyboth, Nucl. Phys. B98 (1975) 93.

[7] P. Darriulat, E. Gygi, M. Holder, K.T. McDonald, H.G. Pugh, K. Tittel and F. Schneider, Conversion efficiency of lead for 30—200 MeV photons, submitted to Nucl. Instr.

[8] G. Neuhofer, F. Niebergall, J. Penzias, M. Regler, K.R. Schubert, P.E. Schumacher, W. Schmidt-Parzefall and K. Winter, Phys. Letters 37B (1971) 438.

[9] B. Betev, G. Bohm, P. Darriulat, I. Derado, P. Dittmann, V. Eckardt, K. Eggert, H.J. Gebauer, M. Holder, K.T. McDonald, R. Meinke, T. Modis, H.G. Pugh, O.R. Sander, P. Seyboth, W. Thomé and K. Tittel, Observation of proton-proton interactions with π^0 of large transverse momentum at the ISR, paper submitted to the 17th Int. Conf. on high-energy physics, London, 1974;
L. Di Lella, rapporteur's talk, Proc. 17th Int. Conf. on high-energy physics, London, 1974 (Rutherford Lab., Chilton, Didcot, 1974) p. V-13.

[10] G. Finocchiaro, P. Grannis, H. Jöstlein, R. Kephart, R. Thun, G. Bellettini, P.L. Braccini, R. Castaldi, T. Del Prete, P. Laurelli, A. Sanguinetti and M. Valdata, Charged particle multiplicities associated with large transverse momentum photons at the ISR, paper submitted to the 17th Int. Conf. on high-energy physics, London, 1974;
P.V. Landshoff, Proc. 17th Int. Conf. on high-energy physics, London, 1974 (Rutherford Lab., Chilton, Didcot, 1974) p. V-57.

[11] G. Finocchiaro, P. Grannis, D. Green, H. Jöstlein, R. Kephart, R. Thun, S.R. Amendiola, G. Bellettini, P.L. Braccini, C. Bradaschia, R. Castaldi, C. Cerri, T. Del Prete, L. Foa, P. Giromini, P. Laurelli, A. Menzione, L. Ristori, G. Sanguinetti and M. Valdata, Phys. Letters 50B (1974) 396.

[12] F.W. Büsser, L. Camilleri, L. Di Lella, B.G. Pope, A.M. Smith, J.K. Yoh, B.J. Blumenfeld, L.M. Ledermann, R.L. Cool, L. Litt and S.L. Segler, Phys. Letters 51B (1974) 306.

[13] F.W. Büsser, L. Camilleri, L. Di Lella, B.G. Pope, A.M. Smith, B.J. Blumenfeld, S.N. White, A.F. Rothenberg, S.L. Segler, M.J. Tannenbaum, M. Banner, J.B. Chèze, H. Kasha, J.P. Pansarts, G. Smadja, J. Teiger, H. Zaccone and A. Zylberstejn, Phys. Letters 55B (1975) 232.

[14] B. Alper, H. Bøggild, P. Booth, L.J. Carroll, G. von Dardel, G. Damgaard, B. Duff, J.N. Jackson, G. Jarlskog, L. Jönsson, A. Klovning, L. Leistam, E. Lillethun, S. Olgaard-Nielsen, M. Prentice and J.M. Weiss, Nucl. Phys. B87 (1975) 19.

[15] K. Eggert, H. Frenzel, W. Thomé, B. Betev, P. Darriulat, P. Dittmann, M. Holder, K.T. McDonald, T. Modis, H.G. Pugh, K. Tittel, I. Derado, V. Eckardt, H.J. Gebauer, R. Meinke, O.R. Sander and P. Seyboth, Nucl. Phys. B86 (1975) 201.

[16] A.P. Contogouris and D. Schiff, Correlations at large transverse momenta, CERN preprint TH.2029 (1975), Phys. Letters, to be published.